Numerical study on fiber waviness defect and sensitivity analysis of the parameters

Long Zhou*, and *Shuhua* Zhu

Nanjing University of Aeronautics and Astronautics, Nanjing, China

Abstract. The presence of fiber waviness defects is well-known to reduce the compressive strength. A FE model was established and the results of failure load and mode were compared with the test results to demonstrate the validity and accuracy. The influence of two parameters L and offset Angle θ of fiber waviness defect was studied. The simulation results show that the compression failure load increases with the increasing of L at constant A/H for convex and concave fiber fold by 33.0% and 20.1% respectively, but there is no significant effect on the failure load with θ within 5%.

1 Introduction

Composite laminates are more susceptible to manufacture defects due to their inherent anisotropic characteristics of composite materials and complex manufacture processes. Fiber waviness defects are the commonly observed manufacture defects in the composite laminates, which was introduced unintentionally during manufacturing process. The presence of fiber waviness defects is well-known to reduce the compressive strength of composite laminates. Therefore, the investigations of fiber waviness defects are important both to evaluate the structural integrity of composite components, and to improve manufacture techniques to reduce the defects.

Many studies have been done on the fiber waviness defects, which were introduced unintentionally during manufacturing process. Chan et al. [1] studied the influence of fiber waviness on the deflection and natural frequency of symmetric composite beams. Mukhopadhyay et al. [2] conducted compression tests and numerical simulations on artificially induced fiber waviness. Bloom [3] and El-Hajjar [4] et al. studied the influence of fiber waviness on the strength and failure mode of laminates through tensile test. Kugler et al. [5] determined the material and process parameters that have the greatest influence on the development of waviness in laminates, and explained the influence emphases of different parameters. Potter et al. [6] investigated how different choices in composite design affect the performance of composite materials and induce defects. Lightfoot et al. [7] proposed a new waviness formation mechanism based on the shear force caused by the mismatch of thermal expansion coefficient between composite materials and tools, and the interlayer slip process occurring during consolidation.

* Corresponding author: zhoulong@nuaa.edu.cn

A lot of experimental and numerical studies have been carried on the mechanical performance of the composite laminates and structures with fiber waviness. Xu et al. [8] studied the influence of out-of-plane waviness on full-thickness tensile strength through experiments and numerical studies on multidirectional curved beam laminate, and the strength could be reduced by 16%. Hu et al. [9] also studied bending composites. Predefined waviness profiles were generated using special lay-up and forming processes, and mechanical tests and DIC measurements were performed to illustrate the effect of the waviness. It is found that local stress concentration around waviness is an important factor leading to failure. Alves et al. [10] collated and compared the analytical methods developed to predict mechanical properties. Based on the latest techniques in this field of research, they studied and debated specially formulated experimental techniques to investigate the effect of corrugations on key structural characteristics.

There have been many experimental and simulation studies on laminates with fiber waviness defect, but few of them were referred to the parameter sensitivity of the waviness. In this paper, an accurate finite element model was established to explore the impact of length L and offset angle θ.

2 Finite element model

2.1 Theory of failure criterion

2.1.1 CFRP plies

The strength theory of composite takes into account damage characterization, stress analysis, damage judgment and damage evolution. The Continuum Damage Mechanics (CDM) holds that material damage will directly result in the reduction of carrying capacity. It provides a method that can accurately determine the full range of deterioration in a composite material [11]. Based on CDM, Puck's theory [12,13] was coded as VUMAT subroutines in ABAQUS/Explicit which assumes that the brittle fracture of the matrix in unidirectional composite lam-inates will generate a crack plane parallel with the fiber direction (Figure 1).

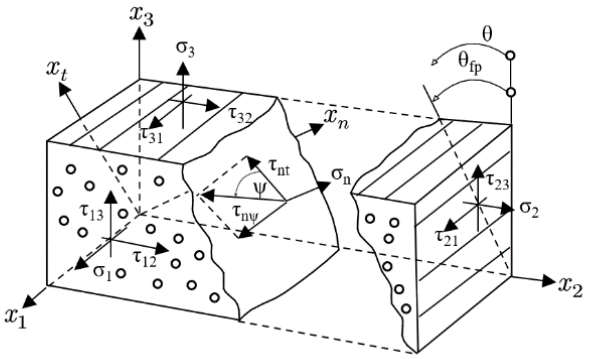

Fig. 1. Cross section of specimens containing a fiber waviness defect.

In Puck's Definition of stresses on the crack plane theory, the material fracture is represented by the stress exposure f_E. If f_E <1, there is no damage, otherwise if $f_E \geqslant 1$, the material has damage occurred. Besides, Puck considered that fiber failure (FF) and inter-

fiber failure (IFF) must be treated by different criteria. According to the IFF hypothesis, two different fracture conditions for IFF are required as shown in Equation 1.

$$f_{E_{IFF}}(\theta)=\begin{cases}\left[\left(\frac{1}{R_{\perp}^{t}}-\frac{p_{\perp\psi}^{t}}{R_{\perp\psi}^{A}}\right)^{2}\sigma_{n}^{2}(\theta)+\left(\frac{\tau_{nt}(\theta)}{R_{\perp\perp}^{A}}\right)^{2}+\left(\frac{\tau_{nl}(\theta)}{R_{\perp\parallel}}\right)^{2}\right]^{\frac{1}{2}}+\frac{p_{\perp\psi}^{t}}{R_{\perp\psi}^{A}}\sigma_{n}(\theta),\left(\sigma_{n}(\theta)\geq 0\right)\\ \left[\left(\frac{p_{\perp\psi}^{c}}{R_{\perp\psi}^{A}}\sigma_{n}(\theta)\right)^{2}+\left(\frac{\tau_{nt}(\theta)}{R_{\perp\perp}^{A}}\right)^{2}+\left(\frac{\tau_{nl}(\theta)}{R_{\perp\parallel}}\right)^{2}\right]^{\frac{1}{2}}+\frac{p_{\perp\psi}^{c}}{R_{\perp\psi}^{A}}\sigma_{n}(\theta),\left(\sigma_{n}(\theta)<0\right)\end{cases} \tag{1}$$

2.1.2 Cohesive interfaces

The interfaces were modelled using a 3D cohesive interface constitutive in the traction-separation law embedded in Abaqus/Explicit. The opening (mode I) and sliding (mode II) displacements between the top and bottom surfaces of the cohesive element were related to the corresponding stress components by high interfacial stiffness value KI and KII. The material parameters of the cohesive zones are given in Table 3. The cohesive interfacial stiffness and strength were estimated because they cannot be measured directly. The quadratic stress criterion was used to detect damage initiation

$$\left(\frac{\langle\sigma_{nn}\rangle}{N_{max}}\right)^{2}+\left(\frac{\sigma_{ss}}{S_{max}}\right)^{2}+\left(\frac{\sigma_{tt}}{T_{max}}\right)^{2}=1 \tag{2}$$

where σ_{nn} is the normal component of stress in the cohesive layer, σ_{ss} and σ_{tt} are two shear traction components of stress in cohesive layer, while N_{max}, S_{max} and T_{max} are the mode I, mode II and mode III failure initiation stresses. Here, the Macaulay bracket on σ_{nn} indicates that negative normal traction component does not contribute to traction-separation of cohesive layer. After damage initiation is detected at the interface, the bilinear damage evolution law is used to degrade the stiffness of the cohesive elements. The damage variable ddelam was defined by

$$d_{delam}=\max\left\{0,\min\left\{1,\frac{\delta_{m}-\delta_{m}^{i}}{\delta_{m}^{f}-\delta_{m}^{i}}\right\}\right\} \tag{3}$$

where δ_m is the effective displacement in interfacial mixed-mode. The superscript 'i' and 'f' indicate their values corresponding to damage initiation and complete failure, respectively. The damage variables d_{delam} was used to degrade the interfacial stiffness linearly from 0 (no damage) to 1 (complete failure) following a mixed-mode delamination. After damage initiation, a power law fracture energy criterion was used for the damage evolution.

2.2 Modelling in abaqus

The composite laminates specimens were designed containing different severity of fiber waviness. The stacking sequence is $[45/0/-45/90/45/0/-45/0/45/0]_s$. The nominal cured thickness of each ply is 0.19mm. The nominal total thickness of the specimens is 3.8mm. All the specimens were machined in the length of 140mm and the width of 12mm. The unsupported length of the specimens was 12mm.

The severity of the fiber waviness defect is illustrated in Fig. 2. The nominal thickness of laminates is defined as H. The maximum depth of dent or height of convex is defined as A. The severity of the dent defect is characterized by the fiber waviness ratio *A/H*. Four

configurations of specimens with different fiber waviness ratios were investigated, which were 10%, 20%, -10%, -20%, respectively, where the negative sign represents the concave waviness of the fiber, otherwise it is the convex waviness of the fiber.

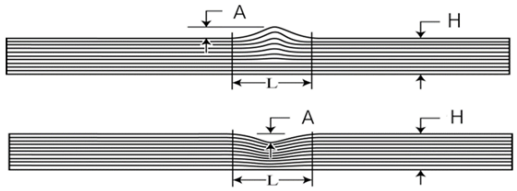

Fig. 2. Cross section of specimens containing a fiber waviness defect.

The plies of composite were modelled using 3D 8-noded solid reduced-integration elements (C3D8R). There were one layer elements in the thickness direction of each ply. The "enhanced" hourglass control option was used to avoid the appearance of spurious zero-energy hourglass modes in the reduced integration C3D8R elements. Zero thickness 8-noded cohesive COH3D8 elements were inserted among all the plies to model delamination failure. Fine mesh, 0.25×0.25mm in-plane dimension, was employed in the concave fiber waviness containing zone. Otherwise, a relatively coarser grid, the largest size scale reached to 0.75×0.25mm in-plane dimension, was used in the other zones to improve the efficiency of calculation. A typical FE model of specimen consisted of 34560 C3D8R elements and 32832 COH3D8 elements. The mesh of typical specimen and the actual side view of specimen were presented in Fig. 3.

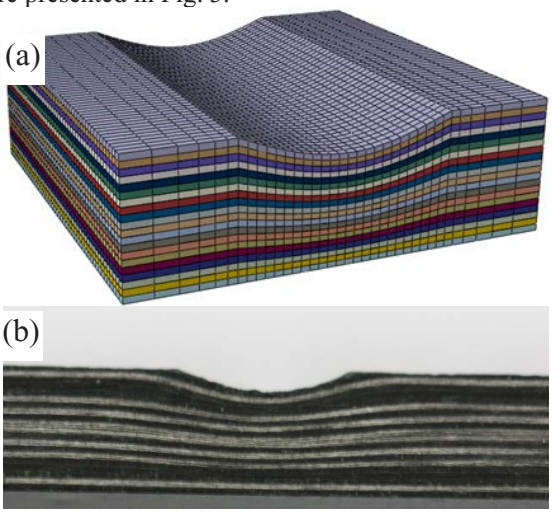

Fig. 3. FE mesh and actual side view of specimen with concave fiber waviness specimen (a) FE mesh of specimen (b) side view of test specimen.

The finite element models were built in Abaqus/Explicit with quasi-static analysis and the explicit dynamic solver. The calculated kinematic energy was less than 5% of internal energy of model, which indicated that the quasi-static simulation was credible. In order to improve the computing efficiency, only the gauge length of 12mm of the specimens were modelled. The fiber waviness is defined as the cosine function in the thickness direction with a wavelength of λ and an amplitude of $2a$.

The scanning of the convex fiber waviness shows that the fibers of the lower half composite laminate had no waviness along the through-thickness direction of the specimens, while the upper-half fibers had waviness along the through-thickness di-rection. The nodal

coordinates of the convex fiber waviness model in the direction of through-thickness are defined as:

$$Z_W = Z_0 + \Delta Z \tag{4}$$

where Z_W is the nodal coordinate of the through-thickness direction of the fiber waviness model, Z_0 is the nodal coordinate of the through-thickness direction of the waviness-free model and ΔZ is expressed as:

$$\Delta Z = \begin{cases} \left(\operatorname{sgn}\left(z-\frac{H}{2}\right)+1\right)\frac{BT}{2}\frac{A}{H}\cos\left(\frac{2\pi}{\lambda}\right) & if\ -\frac{\lambda}{4} \le x \le \frac{\lambda}{4} \\ 0 & otherelse \end{cases} \tag{5}$$

Note that sgn(x) is the symbolic function:

$$\operatorname{sgn}(x) = \begin{cases} 1 & x > 0 \\ 0 & x = 0 \\ -1 & x < 0 \end{cases} \tag{6}$$

where x is the coordinate of the model length direction. λ is the wavelength of the waviness, and the wavelength of the fiber waviness on the specimens is half the wave-length. A is the convex height of the fiber waviness in the direction of through-thickness, and H is the theoretical thickness of the model. B is the amplitude in the direction of through-thickness, which is one on the top surface of the FE model, linearly decays in the direction of through-thickness, and takes to zero at the middle-plane position of the composite laminates. T is equivalent to H, which is also the thickness of the model. A/H is used here to define the severity of fiber waviness.

For the geometrical profile of the concave fiber waviness, it is roughly the same as that of the convex fiber waviness model. The curvature of the concave fiber waviness gradually decays from the top surface to its subsequent plies. Therefore, the severity of the concave fiber waviness on the top layer was the largest, and the bottom layer did not have any fiber waviness. The nodal coordinate of the concave fiber waviness model in the through-thickness direction is defined as follows:

$$Z_w = Z_0 - \Delta Z \tag{7}$$

and ΔZ is expressed as:

$$\Delta Z = \begin{cases} \frac{BT}{2}\frac{A}{H}\cos\left(\frac{2\pi}{\lambda}\right) & if\ -\frac{\lambda}{4} \le x \le \frac{\lambda}{4} \\ 0 & otherelse \end{cases} \tag{8}$$

Note that the meanings of symbols in Equation (7) are identical to those in the convex fiber waviness model. In the concave fiber waviness model, parameter B is one at the top layer and zero at the bottom layer.

3 Numerical results and verification

The material properties of the T800/epoxy composite were used in this study. The failure loads of the specimens predicted by finite element analysis are summarized in Table. 1. It can be seen that the errors of experimental values and simulation values of other specimens are within 10%.

Table. 1. Experimental and simulation results of fiber waviness specimens.

A/H	Simulation Value/kN	Experimental value /kN	Error
0%	34.86	36.53	−4.57%
−20%	14.08	15.27	−7.79%
−10%	21.85	23.21	−5.86%
10%	26.16	26.55	−1.47%
20%	24.39	24.73	−1.37%

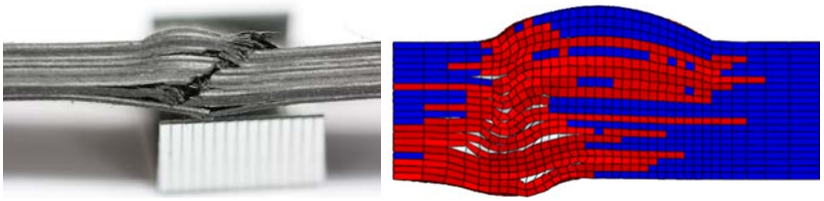

(a) **(b)**

Fig. 4. Typical failure mode (a) compression test (b) FE model.

Fig. 4 shows the test and simulation failure mode of typical specimens with fiber waviness, where the defects are on the top of the pictures. The elements in blue are the undamaged regions. The elements in red are the failure regions. The elements in white are the delamination regions. By comparing (a) and (b) in Fig. 4, it can be found that the failure mode of the fiber waviness model obtained by finite element simulation is similar to the failure situation of the experiment, and most of the failure occurs at the maximum dislocation Angle. This is also the aera where the stress is easy to concentrate and the fragile part of the fiber waviness specimens. The experimental failure load and failure mode are close to the simulation results, which shows the validity and accuracy of the finite element model from both sides.

4 Sensitivity analysis of related parameters

4.1 Length of fiber waviness

In section 4, the length of fiber waviness *L* along the length direction of specimens is constant. In this part the influence of L is studied when A/H is 10% or -10%. L varies from 3mm to 6mm and the interval is 1mm both in concave and convex fiber waviness. The results are shown in Table. 2 and Fig. 5.

Table. 2. Simulation results of fiber waviness specimens with *L*.

A/H	*L*	Simulation Value/kN
10%	3	20.91
10%	4	23.75
10%	5	24.51
10%	6	26.16
−10%	3	14.64
−10%	4	16.83
−10%	5	19.67
−10%	6	21.85

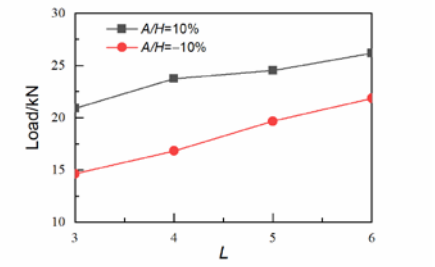

Fig. 5. Simulation results of fiber waviness specimens with different L.

The curves presented in Fig. 5 decreases with the decrease of *L* in both cases where fiber waviness is concave or convex. Although simply reducing the value of *L* under the condition that *A/H* remains unchanged will reduce the area affected by fiber waviness defects in the working section of the specimens, it will increase the fold angle, leading to more concentrated stress and reduced bearing capacity. When *L* is 3mm, their failure modes of FE models are the same as when *L* is 6mm, but the load decreases by 20.1% in the case of concave waviness and 33.0% in the case of convex waviness, indicating that L has a significant impact on fiber waviness.

4.2 Offset angle of fiber wavines

The fiber waviness defects discussed in the previous paper are perpendicular to the length direction of the sample, that is, the offset angle is 90°. In the actual manufacturing process, fiber waviness defects may show other angles as shown in Fig. 6. In this part the influence of offset angle θ is studied when A/H is 10% or -10%. θ varies from 90° to 70° and the interval is 5° both in concave and convex fiber waviness. The results are shown in Table. 3 and Fig. 7.

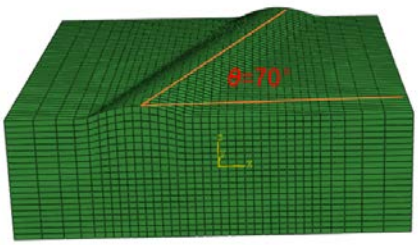

Fig. 6. Fiber waviness defects with θ=70°.

Table. 3. Simulation results of fiber waviness specimens with θ.

A/H	θ	Simulation Value/kN
10%	90°	20.91
10%	85°	21.21
10%	80°	21.44
10%	75°	21.67
10%	70°	21.61
−10%	90°	14.64
−10%	85°	14.86
−10%	80°	15.07
−10%	75°	15.44
−10%	70°	15.41

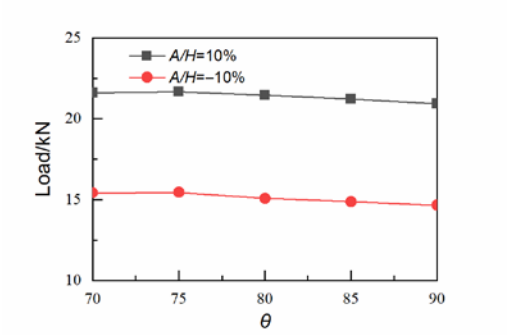

Fig. 7. Simulation results of fiber waviness specimens with different θ.

It can be seen from Fig. 7 that the two curves tend to be basically horizontal. During the change process of θ from 90° to 70°, the failure load changes slightly within 5%. Fig. 8 shows the typical failure mode of fiber waviness defects specimens with offset angles. At the initial stage of damage, fiber damage occurs at the maximum angle of the waviness, as shown in (a). Then, with the loading of compression load, a large number of layered failure occurs in the area affected by the wrinkle, as shown in (b). In spite of the change of offset angle, the number and degree of fiber wrinkling are not changed, and the stress concentration at the waviness is basically unchanged, so the bearing capacity of laminates does not decrease. It can be concluded that the offset angle of fiber waviness defects only has slight effect.

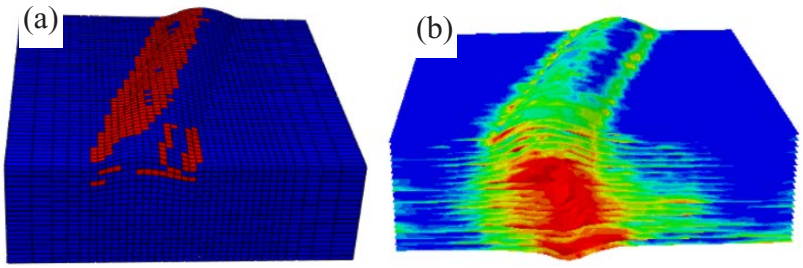

Fig. 8. Failure mode of fiber waviness defects with offset angle.

References

1. WS. Chan and JS. Wang, Influence of fiber waviness on the structural response of composite laminates, Journal of Thermoplastic Composite Materials., **3** (1994)
2. S. Mukhopadhyay, M. Jones and S. Hallett, Compressive failure of laminates containing an embedded wrinkle; experimental and numerical study, Composites Part A: Applied Science and Manufacturing., **73** (2015)
3. L. Bloom, J. Wang and K. Potter, Damage progression and defect sensitivity: An experimental study of representative wrinkles in tension, Composites Part B: Engineering., **45** (2013)
4. R. El-Hajjar and D. Petersen, Gaussian function characterization of unnotched tension behavior in a carbon/epoxy composite containing localized fiber waviness, Composite Structures., **93** (2011)
5. D. Kugler and T. Moon, Identification of the most significant processing parameters on the development of fiber waviness in thin laminates., Journal of Composite Materials., **36** (2002)

6. K. Potter, B. Khan and M. Wisnom et al, Variability, fiber waviness and misalignment in the determination of the properties of composite materials and structures, Composites Part A: Applied Science and Manufacturing., **39** (2008)
7. J. Lightfoot, M. Wisnom and K. Potter, A new mechanism for the formation of ply wrinkles due to shear between plies, Composites Part A: Applied Science and Manufacturing., **49** (2013)
8. X. Xu, M. Jones and H. Ali, et al, Effect of out-of-plane wrinkles in curved multi-directional carbon/epoxy laminates, Composites Science and Technology., **197** (2020)
9. H. Hu, D. Cao and Z. Cao, et al, Experimental and numerical investigations of wrinkle effect on failure behavior of curved composite laminates, Composite Structures., **261** (2021)
10. M. Alves, C. Junior and S. Ha, Fiber waviness and its effect on the mechanical performance of fiber reinforced polymer composites: an enhanced review, Composites Part A., **149** (2021)
11. B. Falzon and P. Apruzzese, Numerical analysis of intralaminar failure mechanisms in composite structures. Part I: FE implementation. Composite Structures , **93** (2011)
12. A. Puck and M. Mannigel, Physically based non-linear stress–strain relations for the inter-fibre fracture analysis of FRP laminates. Composites Science and Technology, **67** (2007)
13. M. Knops, Analysis of failure in fiber polymer laminates - The Theory of Alfred Puck, Springer, Berlin, Heidelberg (2008)